Supporting Information

A Key Descriptor for Corrosion Engineering of NiFe-LDH: Unlocking Peak Performance by Managing Fe-ion Concentration

Bohan Deng,[a,b] Kenan Shen,[a] Heyong Zhu,[a] Zheming Wang,[a] Yaning Wang,[b] Kun Zhang,*[b] Kai Huang,*[c] Kaihua Xu*[b] and Peng Du*[a]

[a] Zhejiang Key Laboratory for Island Green Energy and New Materials, School of Materials Science and Engineering, Taizhou University, Taizhou, 318000, Zhejiang, China.

[b] GEM (Shenzhen) Super Green Technology Institute, GEM Co., Ltd., ShenZhen, Guangdong, 518102, China.

[c] School of Physical science and Technology, Beijing University of Posts and Telecommunications, Beijing 100876, PR China.

E-mail: pengdu@tzc.edu.cn (P.D), huang-kai@bupt.edu.cn (K.H), xukaihua@gem.com.cn (K.X), zhangkun@gem.com.cn (K.Z)

Experimental Section

Materials

In this work, Nickel chloride hexahydrate ($NiCl_2 \cdot 6H_2O$, GR, >99%) was purchased from Aladdin. Potassium hydroxide (KOH, 99.99% metals basis, except sodium) was purchased from Macklin. Hydrochloric acid (HCl, 37%) was purchased from Sinopharm. Acetone (CH_3COCH_3, AR, >99.5%) was purchased from Aladdin. Iron foam (1mm thick) was purchased from Suzhou Keshenghe Metal Materials Co. Ltd. Commercial IrO_2/NF electrodes (with IrO_2 loading of 2.5 mg cm^{-2}) were purchased from Sinero Technology Ltd. All of the materials were used as received without any further purification except for special declaration in this work.

Preparation of NiFe-LDH/IF electrodes

NiFe-LDH/IF electrodes were prepared by corroding iron substrates in $NiCl_2$ solution. Briefly, Fe foam substrates were cut into 1 cm × 2 cm pieces and thoroughly washed in acetone and 0.5M hydrochloric acid for 15 min by ultrasonication to remove impurities and the surface oxide layer, then washed with deionized water. Then a piece of Fe foam was immersed in 10 mL of 0.2 M $NiCl_2$ solution for a certain amount of time. After the corrosion process, the resulting NiFe-LDH/IF electrode was thoroughly washed with deionized water and dried in air overnight.

For the preparation of NiFe-LDH/IF-IO electrodes, a piece of Fe foam was immersed in 30 mL of 0.2 M $NiCl_2$ solution for 48 hours, and the corrosion solution was refreshed every 12 hours to control the Fe-ion concentration of the corrosion solution. The remaining preparation processes for NiFe-LDH/IF-IO electrodes were identical to those for NiFe-LDH/IF electrodes.

Material characterizations

Scanning electron microscopy (SEM) images were taken by a Hitachi S-4800 microscope operated at 5 kV. TEM and DF-STEM images were taken by a 2100F transmission electron microscope operated at 200 kV. X-ray diffraction analysis was performed by a Bruker D8 Advanced diffractometer in reflection mode with a scanning speed of 10° min^{-1}. Raman spectra were collected using a confocal Raman microscope (DXR3, Thermo Fisher Scientific) with a wavelength of 532 nm and a power of 5 mW at the objective. X-ray photoelectron spectra were collected using a Thermo Fisher Escalab 250Xi spectrometer equipped with an Al Kα radiation source (1487.6 eV) and hemispherical analyzer with a pass energy of 30.0 eV and energy step size of 0.05 eV. All the XPS spectra were corrected by C 1s peak of 284.8 eV and fitted using XPSPEAK41 software with Gaussian-Lorentzian functions. The Ni and Fe contents of the corrosion solution were measured using an inductively coupled plasma optical emission spectrometer (iCAP pro, Thermo Fisher Scientific).

Electrochemical measurement

All electrochemical tests were carried out on a three-electrode cell connected to an electrochemical workstation (CHI 760E, Shanghai Chenhua Instruments). The geometric area of the working electrode was 1 cm × 0.5 cm and the electrolyte was 1M KOH solution. A graphite rod and a Hg/HgO electrode were used as the counter electrode and the reference electrode, respectively. The measured potential versus Hg/HgO reference electrode in 1 M KOH solution could be converted to the potential versus reversible hydrogen electrode (RHE) by the following equation:

$$E_{RHE} = E_{Hg/HgO} + 0.926\,V \quad (1)$$

The cyclic voltammetry (CV) curves were collected at a scan rate of 5 mV s^{-1}. To preclude interference from the Ni^{2+}/Ni^{3+} oxidation current in the evaluation of electrocatalytic activity towards OER, the data for the Tafel plots were collected by

recording the steady-state potential at the end of the 5-min chronopotentiometric program.

IR corrected by 90% of the solution resistance was employed to eliminate the effect of solution resistance. The resistance was measured by electrochemical impedance spectroscopy (EIS) with high frequency of 100 kHz and low frequency of 0.1 Hz at 0.55 V vs. Hg/HgO. The electrochemically active surface area (ECSA) was fitted by a series of cyclic voltammetry curves at different scan rates varying from 10 ~ 100 mV s^{-1} in the potential range of -0.3 ~ -0.2 V vs. Hg/HgO. To estimate the electrochemically effective Ni^{2+} loading of each sample, the working electrode was first charged at 0.8 V vs. Hg/HgO for enough time, then discharged at 0 V vs. Hg/HgO. The discharge current integral is considered as the effective Ni^{2+} loading. For the stability test, chronopotentiometry was applied at a current density of 100 mA cm^{-2}.

Faradaic efficiency calculation

To determine the Faradaic efficiency, an H-type cell was used to collect the generated oxygen and hydrogen separately via a drainage gas gathering method. The Faradaic efficiency can be calculated as:

$$FE(\%) = \frac{V_{gas} \cdot nF}{V_m \cdot \frac{T}{273.15K} \cdot it} \times 100\% \quad (2)$$

Where V_m refers to the standard molar volume of gas (22.4 L mol^{-1}), T refers to the testing temperature.

The calculation of TOF

The calculation of TOF is based on the assumption that every electrochemically accessible Ni atom serves as an active site. The number of active sites (A) is calculated as:

$$A = \frac{Q}{F} \times N_A \quad (3)$$

where Q is the integrated charge of the effective Ni^{2+} loading from Fig. 2d, while F and N_A are the Faraday constant and the Avogadro constant, respectively. The TOF is then determined by the equation:

$$TOF = \frac{\frac{it}{\alpha F} \times N_A}{A \times t} = \frac{i}{\alpha Q} \quad (4)$$

where i is the OER current at a specific overpotential, and α is the electron transfer number ($\alpha = 4$ for OER).

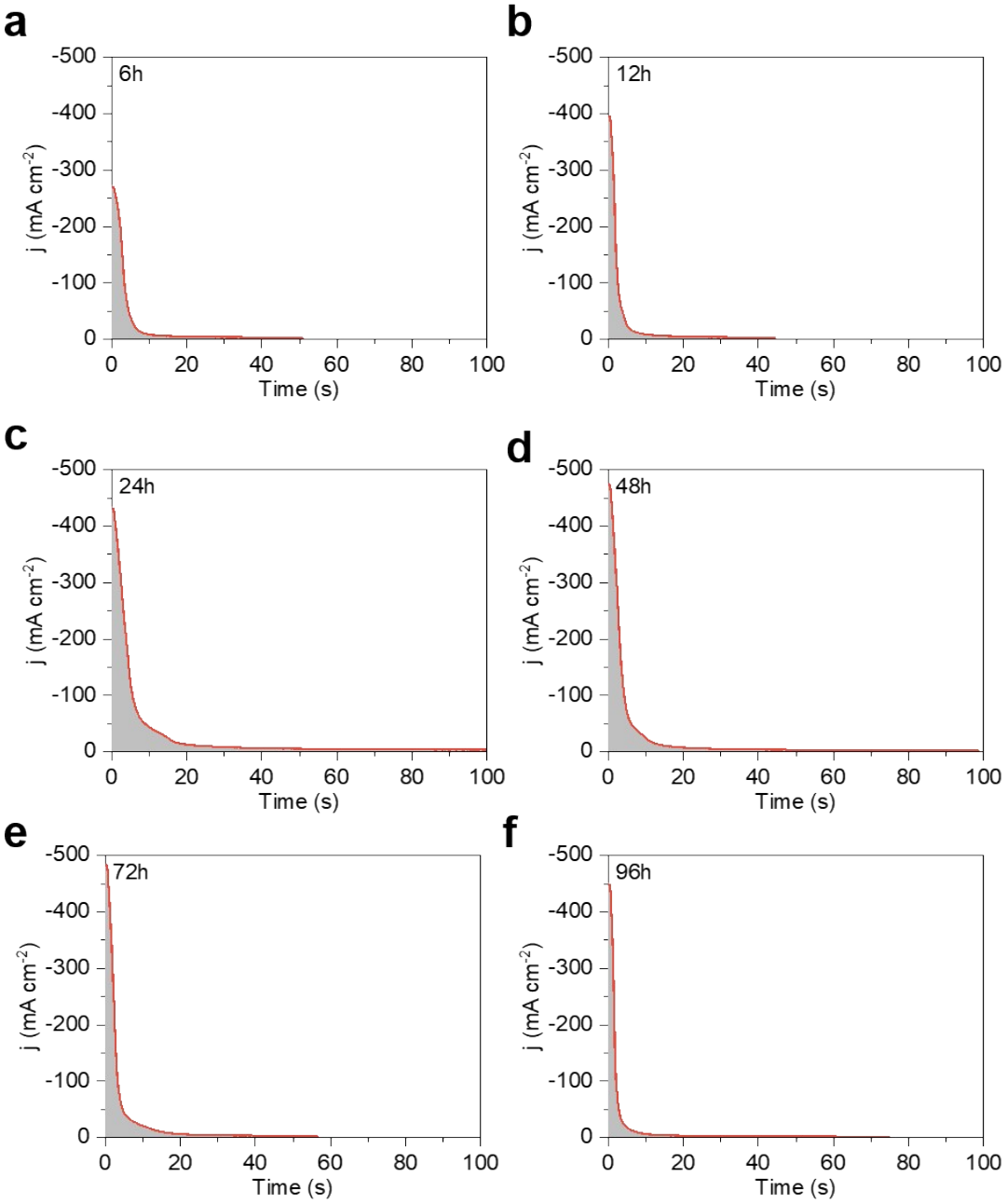

Fig. S1 Chronoamperometric curve at 0 V vs. Hg/HgO for NiFe-LDH/IF electrodes prepared with different corrosion durations: (a) 6 h, (b) 12 h, (c) 24 h, (d) 48 h, (e) 72 h, and (f) 96 h. The NiFe-LDH/IF electrode was fully charged to NiOOH state beforehand. The integrated charge from these curves was used to estimate the effective Ni^{2+} loading.

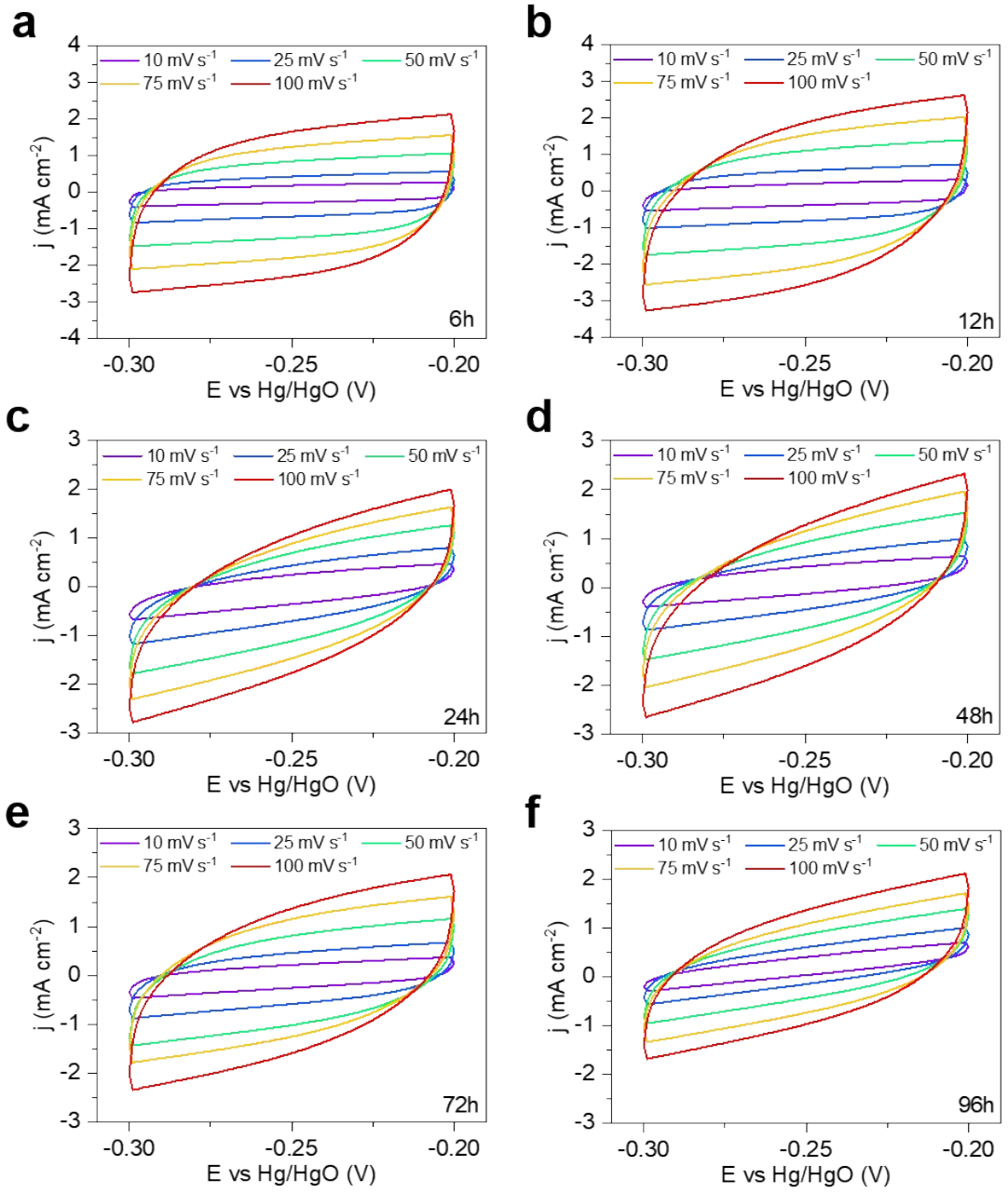

Fig. S2 CV curves of NiFe-LDH/IF electrodes prepared with different corrosion durations: (a) 6 h, (b) 12 h, (c) 24 h, (d) 48 h, (e) 72 h, and (f) 96 h. The measurements were conducted in the non-faradaic potential (-0.3 ~ -0.2 V vs. Hg/HgO) at scan rates of 10, 25, 50, 75, and 100 mV s^{-1}.

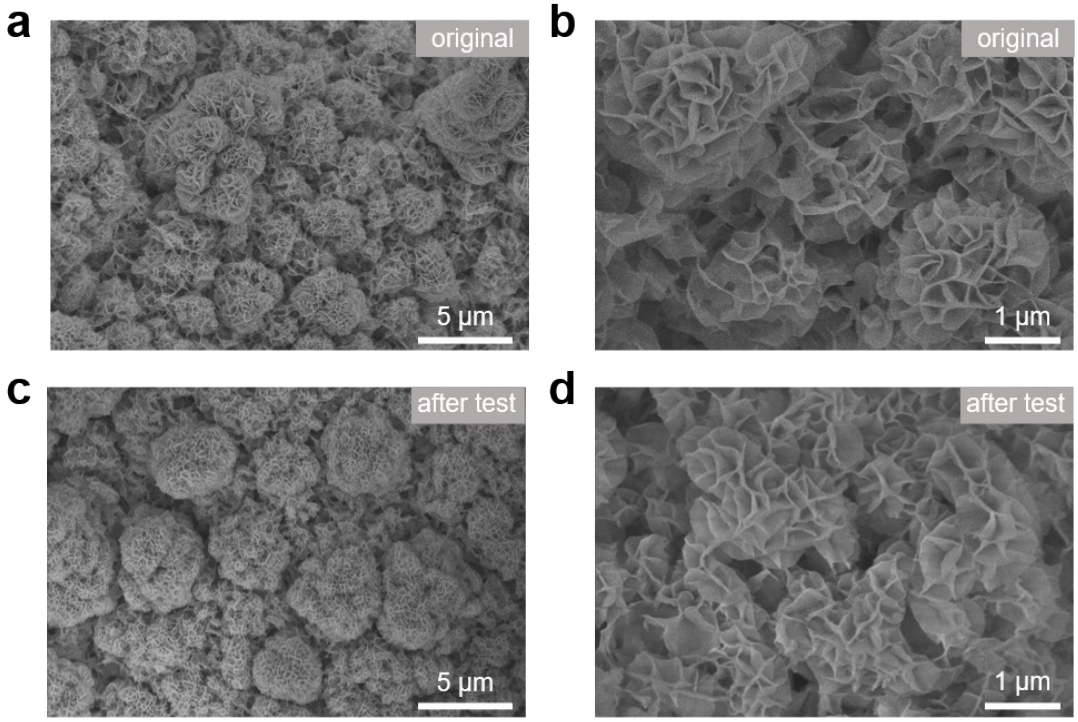

Fig. S3 SEM images of NiFe-LDH/IF-IO (a, b) before and (c, d) after the long-term chronopotentiometric stability test.

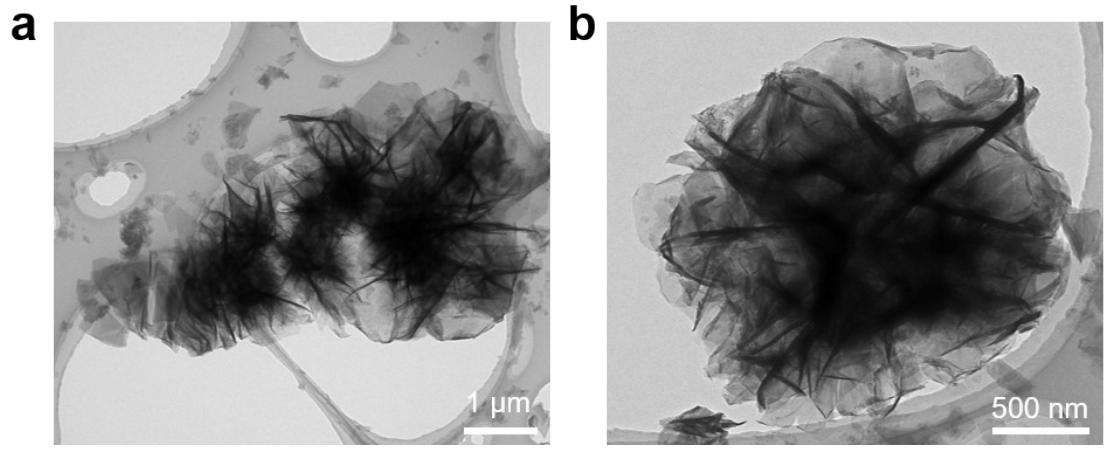

Fig. S4 TEM images of NiFe-LDH/IF-IO at different magnifications.

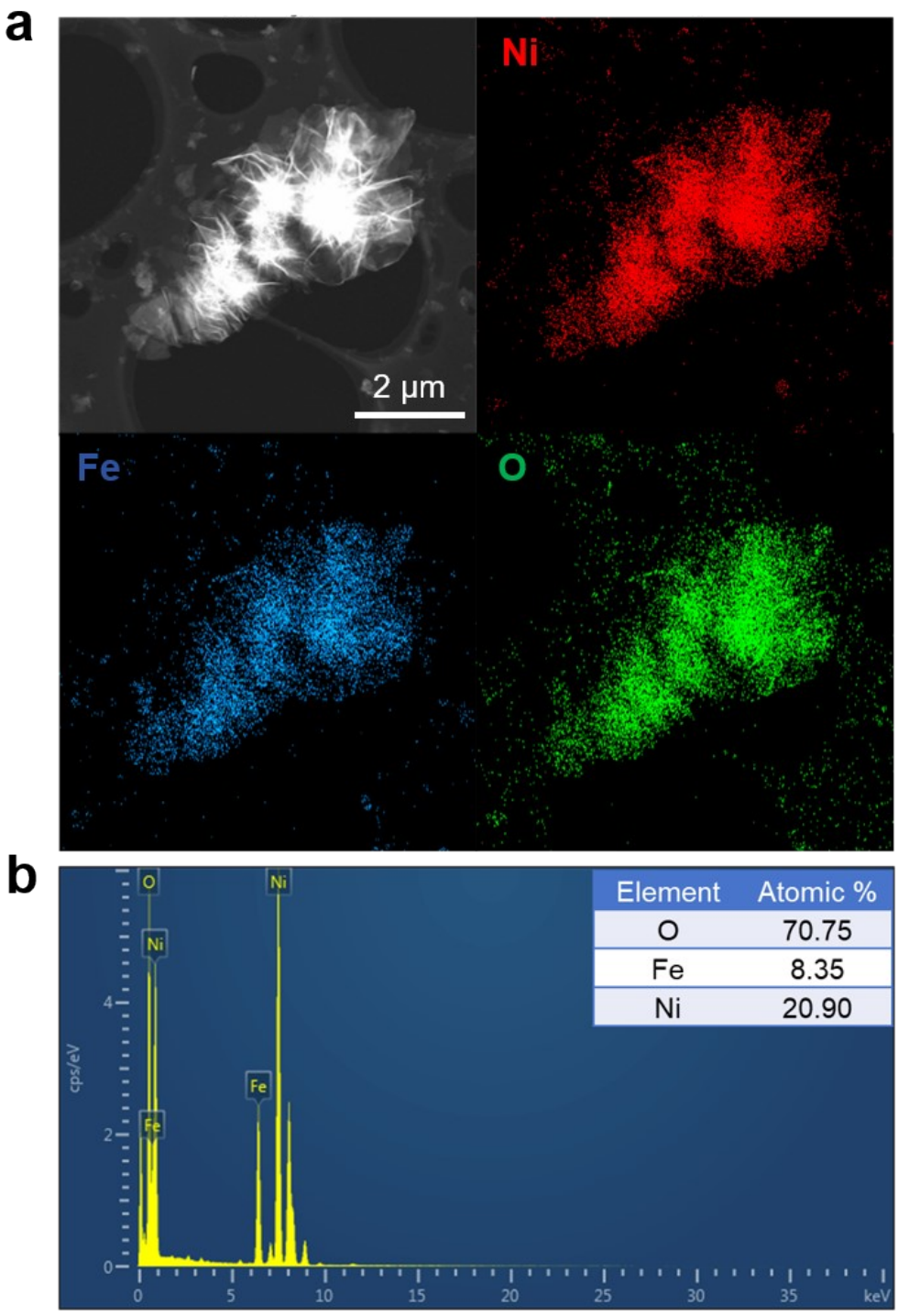

Fig. S5 DF-STEM image of NiFe-LDH/IF-IO and corresponding (a) EDS elemental mapping of Ni, Fe, and O. (b) EDS spectra.

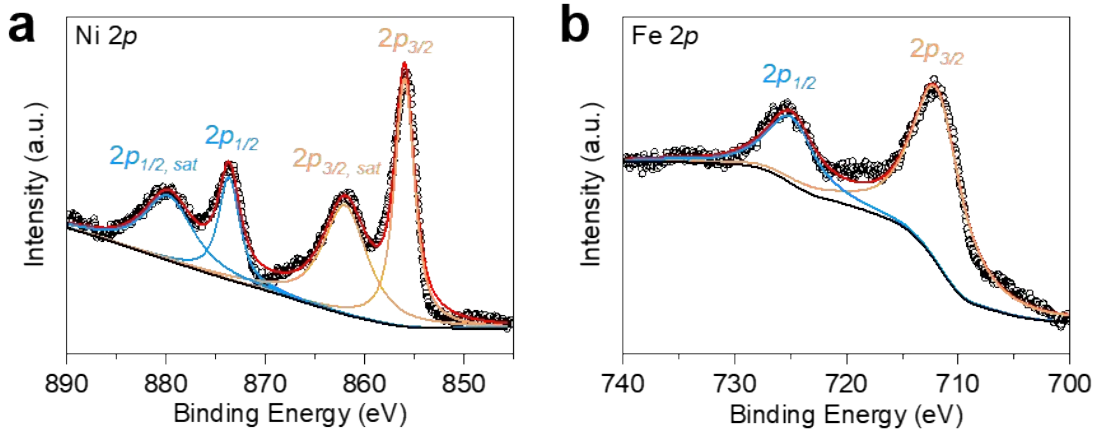

Fig. S6. XPS spectra of NiFe-LDH/IF-IO. (a) Ni 2*p*. Fitted peaks at 855.9 and 873.6 eV were attributed to Ni^{2+} $2p_{3/2}$ and Ni^{2+} $2p_{1/2}$, and peaks at 861.9 and 879.8 eV were their satellite peaks. (b) Fe 2*p*. Fitted peaks at 712.2 and 725.1 eV were attributed to Fe^{3+} $2p_{3/2}$ and Fe^{3+} $2p_{1/2}$, respectively.

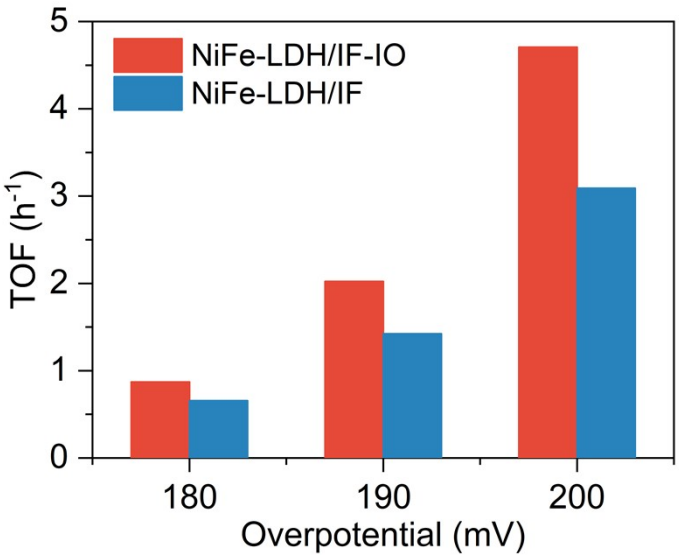

Fig. S7 TOF of NiFe-LDH/IF-IO and NiFe-LDH/IF at various overpotentials.

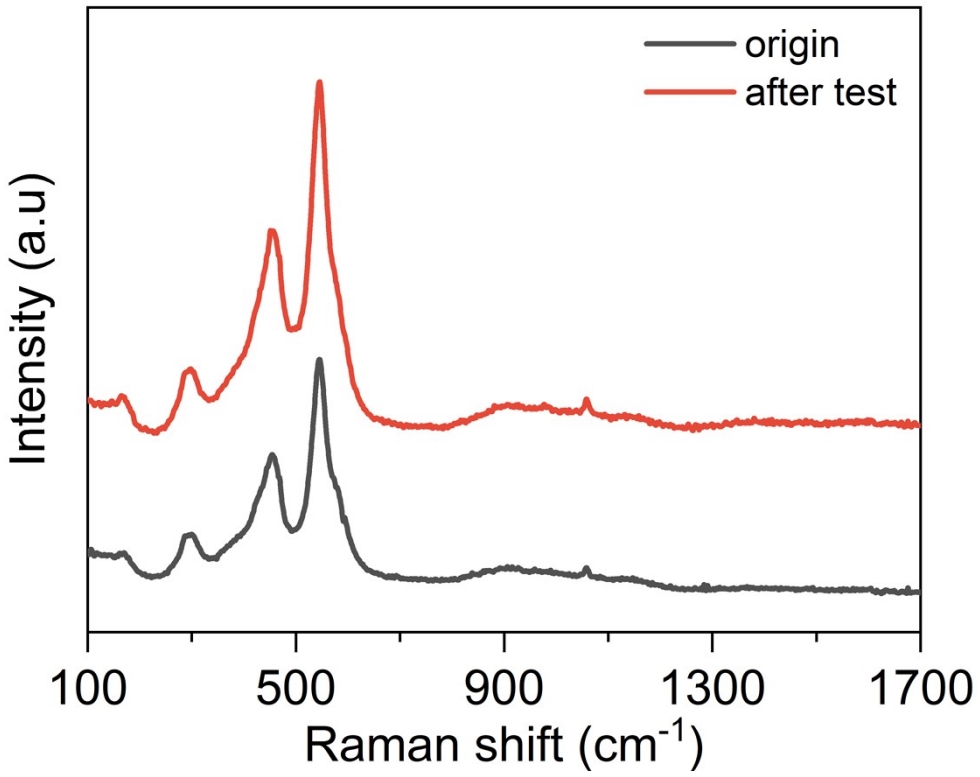

Fig. S8 Raman spectra of NiFe-LDH/IF-IO before and after the long-term chronopotentiometric stability test.

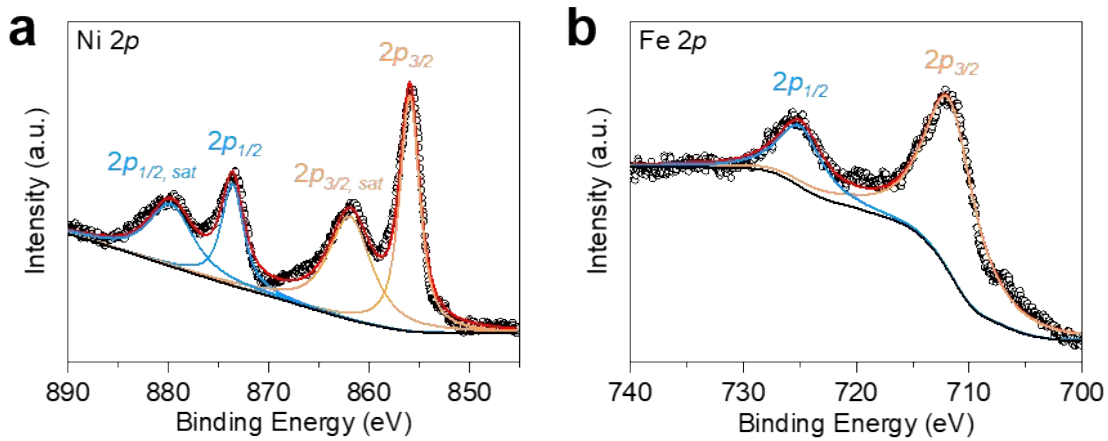

Fig. S9. XPS spectra of NiFe-LDH/IF-IO after the long-term chronopotentiometric stability test. (a) Ni 2*p* (b) Fe 2*p*.

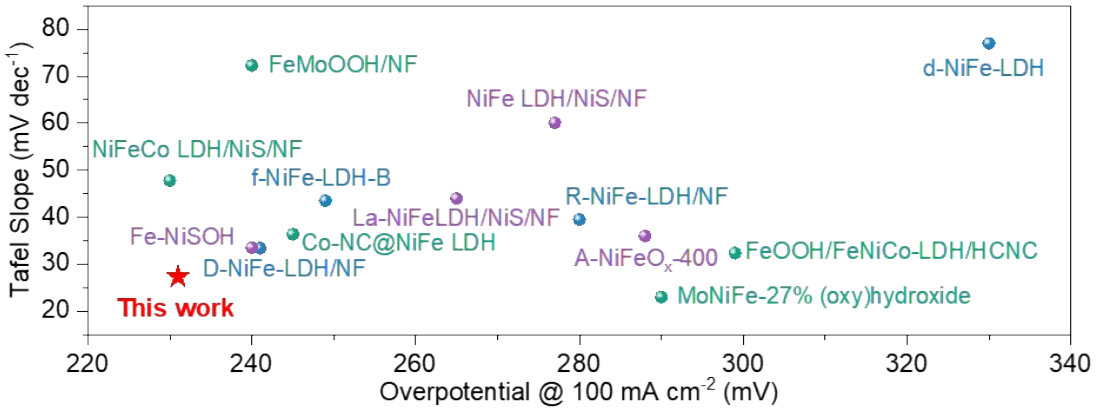

Fig. S10. Comparison of Tafel slopes and overpotentials at 100 mA cm^{-2} for NiFe-LDH/IF-IO and other OER catalysts reported in the previous literature.

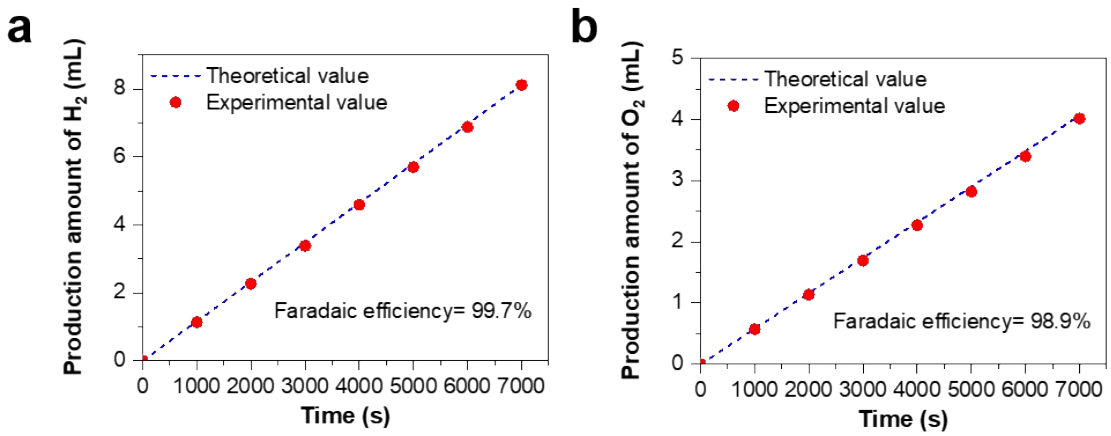

Fig. S11 Faradaic efficiency derived from the experimental yields of (a) H_2 and (b) O_2 at a current density of 10 mA cm^{-2}.

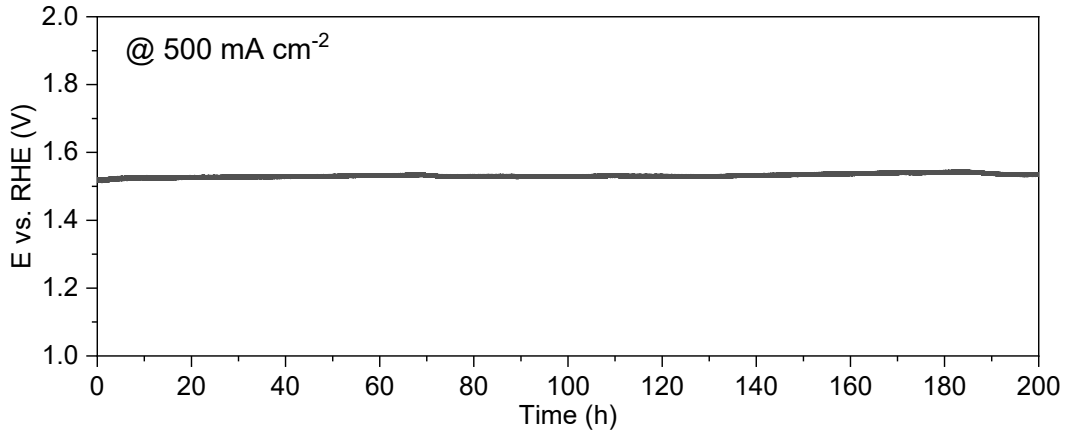

Fig. S12 Long-term stability test of NiFe-LDH/IF-IO at a constant current density of 500 mA cm^{-2}.

Table S1. Optimum fit parameters of the EIS data in Fig. 4e to the equivalent circuit.

Sample	R_s (Ω)	R_f (Ω)	R_{ct} (Ω)
NiFe-LDH/IF-IO	1.85	0.090	1.07
NiFe-LDH/IF	1.94	0.258	1.97

Table S2. Comparison of the NiFe-LDH/IF-IO with other reported OER catalysts in the performance towards water oxidation.

Catalyst	η (mV) @ 10 mA cm^{-2}	η (mV) @ 100 mA cm^{-2}	Tafel slope (mV dec^{-1})	Reference
NiFe-LDH/IF-IO	197	231	27.3	This work
NiFe-LDH/IF	205	244	29.7	This work
R-NiFe-LDH/NF	240	280	39.5	[1]
D-NiFeLDH/NF	209	241	33.4	[2]
d-NiFe-LDH	230	~330	77	[3]
f-NiFe-LDH-B	209	249	43.5	[4]
Fe-NiSOH	207	240	33.5	[5]
La-NiFeLDH/NiS/NF	/	265	44.0	[6]
NiFe LDH/NiS/NF	230	277	60.1	[7]
A-$NiFeO_x$-400	248	288	36	[8]
MoNiFe-27% (oxy)hydroxide	242	290	23	[9]
Co-NC@NiFe LDH	200	~245	36.4	[10]
NiFeCo LDH/NiS/NF	/	230	47.8	[11]
FeOOH/FeNiCo-LDH/HCNC	258	299	32.4	[12]
FeMoOOH/NF	/	240	72.3	[13]

References

1. B. Wang, J. Chen, L. Luo, G. Huang, Q. Shi, Q. Wei, M. Shang and Q. Liu, *Advanced Functional Materials*, 2025, **35**, 2505763.
2. D. K. Cho, H. W. Lim, A. Haryanto, B. Yan, C. W. Lee and J. Y. Kim, *ACS Nano*, 2024, **18**, 20459-20467.
3. Y.-j. Wu, J. Yang, T.-x. Tu, W.-q. Li, P.-f. Zhang, Y. Zhou, J.-f. Li, J.-t. Li and S.-G. Sun, *Angewandte Chemie-International Edition*, 2021, **60**, 26829-26836.
4. S. Zhou, H. He, J. Li, Z. Ye, Z. Liu, J. Shi, Y. Hu and W. Cai, *Advanced Functional Materials*, 2024, **34**, 2313770.
5. C. Huang, Q. Zhou, D. Duan, L. Yu, W. Zhang, Z. Wang, J. Liu, B. Peng, P. An, J. Zhang, L. Li, J. Yu and Y. Yu, *Energy & Environmental Science*, 2022, **15**, 4647-4658.
6. Q. Song, K. Li, Z. Cao, Y. Mi, Q. Kong, G. He, H. liu, Q. Qiao, L. Yao, Y. Wang, X. Dai and X. Zhang, *Chemical Engineering Journal*, 2025, **504**, 157526.
7. Q. Wen, K. Yang, D. Huang, G. Cheng, X. Ai, Y. Liu, J. Fang, H. Li, L. Yu and T. Zhai, *Advanced Energy Materials*, 2021, **11**.
8. Z. Guo, F. Lai, B. Song, S. Wang, H. Singh, P. Talebi, L. Zhu, Y. Niu, G. King, Y. Huang and B. Geng, *Energy & Environmental Science*, 2025, **18**, 8549-8563.
9. Z. He, J. Zhang, Z. Gong, H. Lei, D. Zhou, N. Zhang, W. Mai, S. Zhao and Y. Chen, *Nature Communications*, 2022, **13**.
10. T. Song, H. Xue, J. Sun, N. Guo, J. Sun, Y.-R. Hao and Q. Wang, *Chemical Communications*, 2024, **60**, 972-975.
11. Y. Liu, Q. Song, T. Xu, Q. Kong, G. He, H. Sun, H. Li, Z. Yuan, X. Ma, X. Su, X. p. Dai, Q. Zhang, Z. X. Li, Y. Wei and X. Zhang, *Applied Catalysis B: Environment and Energy*, 2025, **363**, 124811.
12. Y. Luo, Y. Yang, Y. Tian, Q. Wu, W.-F. Lin and M. Wen, *Journal of Materials Chemistry A*, 2025, **13**, 7136-7148.
13. J. Sun, S. Zhou, Z. Zhao, S. Qin, X. Meng, C.-H. Tung and L.-Z. Wu, *Energy & Environmental Science*, 2025, **18**, 1952-1962.